Fabrication and Characterization of Single-Aperture 3.5-MHz BNT-Based Ultrasonic Transducer for Therapeutic Application

Elaheh Taghaddos, T. Ma, Hui Zhong, Qifa Zhou, M. X. Wan, and Ahmad Safari

***Abstract*— This paper discusses the fabrication and characterization of 3.5-MHz single-element transducers for therapeutic applications in which the active elements are made of hard lead-free BNT-based and hard commercial PZT (PZT-841) piezoceramics. Composition of $(BiNa_{0.88}K_{0.08}Li_{0.04})_{0.5}(Ti_{0.985}Mn_{0.015})O_3$ (BNKLT88-1.5Mn) was used to develop lead-free piezoelectric ceramic. Mn-doped samples exhibited high mechanical quality factor (Q_m) of 970, thickness coupling coefficient (k_t) of 0.48, a dielectric constant (ε_{33}^T) of 310 (at 1 kHz), depolarization temperature (T_d) of 200 °C, and coercive field (E_c) of 52.5 kV/cm. Two different unfocused single-element transducers using BNKLT88-1.5Mn and PZT-841 with the same center frequency of 3.5 MHz and similar aperture size of 10.7 and 10.5 mm were fabricated. Pulse-echo response, acoustic frequency spectrum, acoustic pressure field, and acoustic intensity field of transducers were characterized. The BNT-based transducer shows linear response up to the peak-to-peak voltage of 105 V in which the maximum rarefactional acoustic pressure of 1.1 MPa, and acoustic intensity of 43 W/cm^2 were achieved. Natural focal point of this transducer was at 60 mm from the surface of the transducer.**

***Index Terms*— High-power ultrasound (US), piezoelectric and ferroelectric transducer materials, therapeutics, transducer material characterization, and modeling.**

I. Introduction

THE high intensity focused US (HIFU) transducers, with frequencies in a range of 0.5–8 MHz, have widely been used for noninvasive therapeutic procedures such as treatment of benign prostate hyperplasia [1], [2], prostate cancer [3]–[7], breast tumor [8], [9], uterine fibroids [10], [11], liver cancer [12] renal tumor [13], pancreatic cancer [14], and bone metastases [15].

The optimal choice of therapeutic US frequency is application-specific and represents a compromise between treatment depth and the desired rate of heating. Lower frequency transducers are used for deep treatment (e.g., transcranial application) and heat deposition applications, while higher frequency transducers are used for superficial treatments such as prostatic applications [16], [17].

Piezoelectric ceramics with high depolarization temperature, high mechanical quality factor, low dielectric loss, and relatively high coercive field are required for high-power devices such as HIFU transducers. In addition, higher power transmission of US is desirable which is obtained by using low dielectric and mechanical loss materials. It is critical for hard piezoceramics to maintain its low dielectric and mechanical loss at a high vibration velocity under the application of high electric field. Until now, only lead-based piezoelectric compositions such PZT4 and PZT8 have commercially been employed as active elements of HIFU transducers. However, lead is a toxic element which can cause severe health issues for human beings. Therefore, researchers have been trying to develop and characterize hard lead-free composition for high-power applications to protect the environment and public health [18]–[20]. It is reported that the BNT-based ceramics with rhombohedral structure exhibit promising performance under high drive conditions [21]–[24]. Specifically, substitution of B-site (Ti) with Mn in $0.88[Bi_{0.5}Na_{0.5}TiO_3]$-$0.08[Bi_{0.5}K_{0.5}TiO_3]$-$0.04[Bi_{0.5}Li_{0.5}TiO_3]$ (BNKLT88) ceramic resulted in decreasing dielectric loss, the planar coupling coefficient, and dielectric constant. Acceptor dopant ($Mn^{2+,+3}$) considerably enhanced the mechanical quality factor caused by the domain wall pinning effect of oxygen vacancies [19]–[21]. It has been demonstrated that the BNKLT88 ceramics doped with 1.5 mol.% Mn (BNKLT88-1.5Mn) show outstanding high-power performance. Acceptor dopant ($Mn^{2+,+3}$) significantly increased the vibration velocity and suppressed the heat dissipation under high drive condition. Hard Mn-doped lead-free piezoceramics with a maximum vibration velocity (v_{rms}) of 0.6 m/s exhibited superior high-power performance compared to hard commercial PZTs ($v_{\text{rms}} = 0.3-0.5$ m/s) [22], [25], [26].

This paper investigates the performance of hard BNKLT88-1.5Mn piezoceramics for HIFU transducer (HIFU). Here, unfocused lead-free single-element transducer with a center frequency of 3.5 MHz has been prototyped. Pulse-echo response and the acoustic properties of the transducer such as the frequency spectrum, the acoustic pressure field, and the acoustic intensity field were characterized and compared

Manuscript received August 23, 2017; accepted January 9, 2018. Date of publication January 15, 2018; date of current version March 30, 2018. *(Corresponding author: Elaheh Taghaddos.)*

E. Taghaddos and A. Safari are with Glenn Howatt Electroceramic Laboratory, Department of Materials Science and Engineering, Rutgers, The State University of New Jersey, Piscataway, NJ 08854 USA (e-mail: elaheh.taghaddos@rutgers.edu).

T. Ma is with the Paul C. Lauterbur Research Center for Biomedical Imaging Shenzhen Institutes of Advanced Technology, Chinese Academy of Sciences, Shenzhen 518055, China

H. Zhong and M. X. Wan are with the Biomedical Engineering Department, Xi'an Jiaotong University, Xi'an 710049, China.

Q. Zhou is with the Biomedical Engineering Department, National Institutes of Health Resource Center for Medical Ultrasonic Transducer Technology, University of Southern California, Los Angeles, CA 90089 USA.

Digital Object Identifier 10.1109/TUFFC.2018.2793874

to the PZT-based transducer with similar frequency and aperture size. The experimental results demonstrate that BNKLT88-1.5Mn composition is a promising candidate for HIFU transducer applications.

II. Experimental Procedures

A. Preparation and Characterization of the BNT-Based Ceramics

Hard lead-free and lead-based ferroelectric ceramics were used in this paper. The lead-free $(BiNa_{0.88}K_{0.08}Li_{0.04})_{0.5}(Ti_{0.985}Mn_{0.015})$ O_3 composition (abbreviated to BNKLT88-1.5Mn) was prepared in the laboratory setting while the PZT-841 was purchased from APC International, Ltd.

The conventional mixed-oxide method was used to prepare BNKLT88-1.5Mn. High purity precursor ($\geq$99.9%) including oxides and carbonates powders was dried overnight at 120 °C. Then, dried powders were mixed and milled in acetone and yttrium-stabilized zirconium balls for 12 h followed by calcination at 800 °C for 3 h. The procedure continued by milling the calcined powder for 12 h and adding binder (8 wt% Polyvinyl Alcohol solution) to prepare a disk-shaped specimen under 150 MPa uniaxial pressure. Upon binder removal at 550 °C, pellets were sintered at 1100 °C for 2 h. Sintered ceramics were lapped down and then were electroded using high-temperature silver paste. Electroded ceramics were poled in a silicone oil bath at 95 °C under an applied electric field of 45 kV/cm for 15 min. The hard PZT ceramics (PZT-841) has been provided by APC International, Ltd.

The density was calculated based on the dimensions and weight of each sample. The dielectric constant $(\varepsilon_{33}^T/\varepsilon_0)$ and dielectric loss $(\tan\delta)$ were measured at 1 kHz at room temperature by an impedance analyzer (HP4194a; Hewlett Packard, Tokyo, Japan). A Berlincourt piezometer was used to measure the longitudinal piezoelectric charge coefficient (d_{33}) at 100 Hz. The IEEE standards method, resonance and antiresonance frequencies of the impedance traces, has been used to calculate the piezoelectric planar and thickness coupling coefficients (k_p and k_t, respectively) [20], [21], [27]. The longitudinal coupling coefficient k_{33} was estimated from the thickness and planar coupling coefficients according to (1) [28], [29]

$$k_{33}^2 = k_p^2 + k_t^2 - k_p^2 k_t^2. \tag{1}$$

The clamped relative permittivity $(\varepsilon_{33}^s/\varepsilon_0)$ was calculated by the following equation [30]:

$$\varepsilon_{33}^S/\varepsilon_0 = \left(\varepsilon_{33}^T/\varepsilon_0\right)\left[\left(1-k_p^2\right)\left(1-k_t^2\right)\right]. \tag{2}$$

The mechanical quality factor (Q_m) was obtained by the following equation [30]:

$$Q_m = \frac{1}{R}\sqrt{\frac{L}{C_a}} \tag{3}$$

where R, L, and C_a are the resistance, inductance, and capacitance of the Van Dyke equivalent circuit of a piezoelectric resonator at the resonance frequency.

The room temperature polarization-field (P–E) hysteresis loops were measured using a Sawyer-Tower circuit (Radiant Technology Inc., Albuquerque, NM, USA) at a pulse width of 1000 ms (1-Hz frequency) using a triangular wave signal. The dielectric-temperature behavior of the samples was characterized during the heating ramp, within the temperature range of 30 °C–320 °C, by Agilent 4284A Precision LCR Meter.

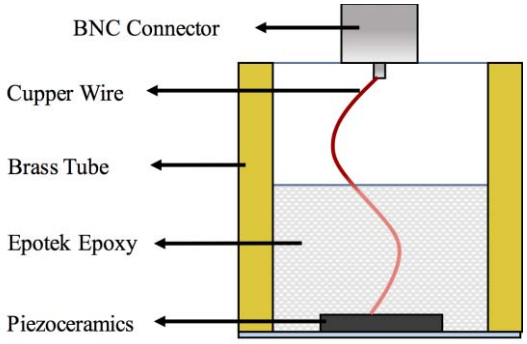

Fig. 1. Schematic illustration of the unfocused ultrasonic transducer.

B. Fabrication and Characterization of Ultrasonic Transducers

A PiezoCAD software (Sonic Concepts Inc., Woodinville, WA, USA) was used to design and predict acoustic performance. In this experiment, we intend to evaluate the performance of unfocused single-element 3.5-MHz BNT-based transducer and compare it to the lead-based transducer with the same frequency and aperture size.

Fig. 1 shows the schematic of the structure of a plain transducer. The BNKLT88-1.5Mn and PZT-841 ceramics with a diameter of 10.7 and 10.5 mm were lapped down to a thickness of 665 and 485 μm, respectively, to achieve the desired resonance frequency of 3.5 MHz. A gold electrode with a thickness of 1000 Å was sputtered on one side of the ceramic to function as the bottom electrode. After attaching the 200-μm wire to the bottom electrode using silver epoxy, the sample was placed inside a brass tube housing. Then the brass tube was filled with Epotek-301 epoxy (Epoxy Technology Inc., Billerica, MA, USA) and was cured at room temperature for 24 h. In order to connect the ceramic to the brass tube, the front side of the transducer was covered by a gold electrode. It should be noted that there were no matching circuit, backing layer, and matching layer on the design of these transducers.

A conventional pulse-echo method in a water tank at room temperature was used to analyze the pulse-echo responses. The transducer was mounted in a tank filled with degassed water and was connected to a variable attenuator and the pulser-receiver (Model 5072R, Panametrics). One cycle of a unipolar signal covering a broadband, 0.5–60 MHz, was used to drive the signal, while a transducer-target distance was set to 55–60 mm from the x-cut quartz target. The bandwidth (BW) of the transducer was calculated by

$$\text{BW} = \frac{f_H - f_L}{f_C} \times 100 \tag{4}$$

where f_c is the center frequency, f_L and f_H are low and high frequencies, respectively, at the -6 dB points of the frequency response spectrum.

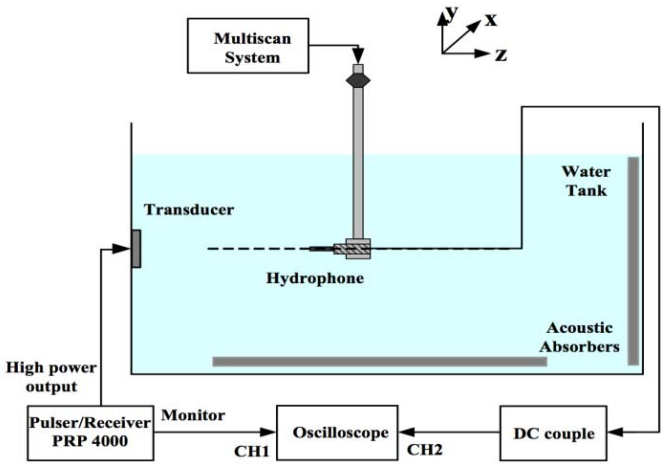

Fig. 2. High-power characterization setup.

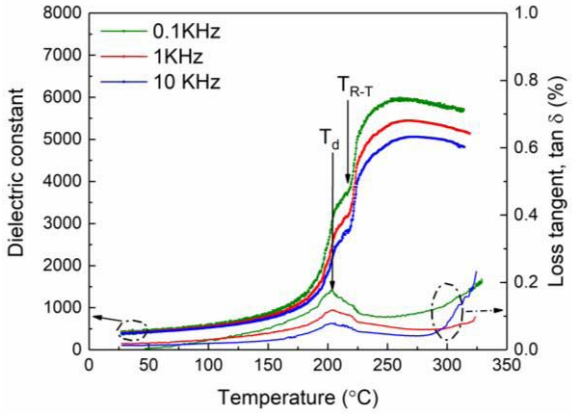

Fig. 3. Temperature dependence of dielectric constant and loss tangent, tanδ (%) of BNKLT88-1.5Mn for poled samples.

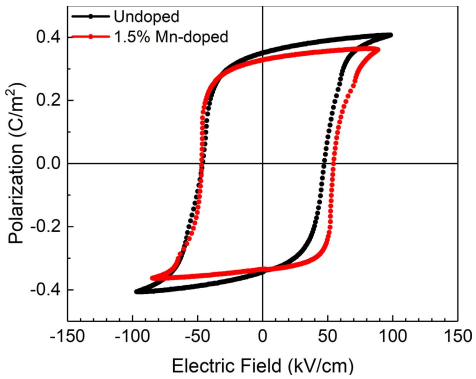

Fig. 4. Polarization-field behavior of undoped and 1.5% Mn-doped BNKLT88 ceramics.

Acoustic characterization set up is shown in Fig. 2. An electric sine-wave pulse with 20 cycles ($n = 20$) generated by Pulse/Receiver PRP4000 (Ritec Inc., Warwick, R.I., USA) provided the transmit waveform to the transducer. The acoustic field was calibrated by a hydrophone-plane-scan method using Multiscan system (C329S, Panametrics Inc., Waltham, MA, USA) with needle hydrophone (0.5-mm diameter; Precision Acoustic Ltd, Dorchester, U.K.). Hydrophone sensitivity was 1109 mV/MPa at 3.5 MHz. The hydrophone scanned the emission field to measure the acoustic pressure and intensity of the transducers in zy-plane (Plane in z- and y-directions). The pulse repetition frequency of 100 Hz and frequency of 3.5 MHz were used for all of the acoustic characterizations.

Spatial peak pulse average intensity (I_{sppa}) and spatial peak temporal average intensity (I_{spta}) calculated by [31]–[33]

$$I_{\text{sppa}} = P^2/2\rho_0\, c_0 \tag{5}$$

$$I_{\text{spta}} = I_{\text{sppa}} \times \text{PD} \times \text{PRF} \tag{6}$$

$$\text{PD} = \frac{n}{f} \tag{7}$$

where P is pressure amplitude *in situ*, ρ_0 is density (ambient density of the medium), c_0 (ambient sound speed), PD is the pulse duration, n is the number of cycles in the pulse, and f is the operating frequency of the transducer.

Output power of the transducer (w_o) and the -6 dB pulse-echo beam diameter ($\text{BD}_{-6\text{ dB}}$) can be evaluated by the following equations:

$$w_o = \frac{\pi \text{BD}_{-6\text{ dB}}^2}{4} I_{\text{spta}} \tag{8}$$

$$\text{BD}_{-6\text{ dB}} = 1.02\, Fc/f\, D \tag{9}$$

in which F is the focal length, c is the material sound velocity, f is the frequency, and D is the diameter of the transducer (active element).

III. Results and Discussion

BNKLT88-1.5Mn has rhombohedral structure at room temperature with complicated phase transitions. The temperature dependence of dielectric constant and loss tangent (tanδ) of poled BNKLT88-1.5Mn at 0.1, 1, and 10 kHz are demonstrated in Fig. 3. Three recognizable anomalies were observed which were related to the depolarization temperature (T_d) close to 205 °C, rhombohedral to tetragonal phase transition at 220 °C, and dielectric maximum temperature (T_m) at 265 °C. The depolarization temperature has been determined by the first peak of temperature-dependent tanδ on heating the poled sample. Deterioration of piezoelectric properties of BNT-based composition occur at T_d and the operating temperature range should be restricted to temperatures lower than T_d. It is worth mentioning that the operating temperature range from lead-based ceramic is limited to Curie temperature (300 °C–320 °C) [34], [35]. In practice, the surface temperature of the transducer does not reach 50 °C which is much lower than T_d of BNT-based ceramic.

Fig. 4 shows the P–E plots for undoped and 1.5 Mn-doped BNKLT88 ceramic. The remanent and saturation polarizations slightly decrease through the acceptor dopant, while the coercive field and the internal bias field (E_i) increase. The alignment of the defect dipoles (e.g., $V_O^{\bullet\bullet}$—$\text{Mn}_{\text{Ti}}^{''}$) in the direction of spontaneous polarization results in the development of internal bias field. The undoped and 1.5% Mn-Doped BNKLT88 ceramics show E_i of 0.7 and 3 kV/cm, respectively. Dielectric and piezoelectric properties of BNKLT88-1.5 Mn ceramic are summarized and compared to hard PZT in Table I.

TABLE I
PROPERTIES OF COMMERCIAL HARD PZTS AND LEAD-FREE BNT-BASED CERAMICS [21], [36]–[40]

Property	PZT4	PZT8	PZT 841	BNKLT88	BNKLT88-1.5Mn
d_{33} (pC/N)	290	225	300	95	85
ε^T_{33}	1300	1000	1375	380	310
tanδ %	0.5	0.4	0.4	1.1	0.85
k_t %	51	48	---	49	48
k_p %	58-64	51-60	60	26	22
Q_m	500	1000	1400	400	970
E_c (kV.cm^{-1})	14	20	---	47.2	52.2
E_i (kV.cm^{-1})	3	3	---	0.7	3
T_c (°C)	328	300	320	~275 (T_m)	265 (T_m)
T_d (°C)	---	---	---	~220	205

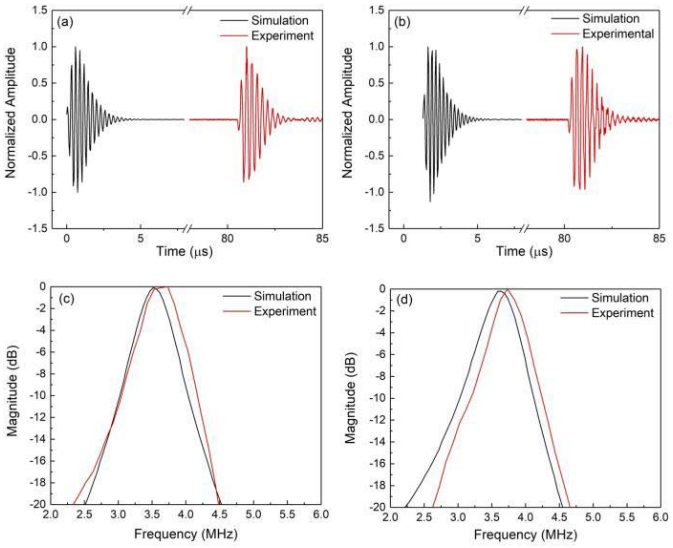

Fig. 5. (a)–(d) Time and frequency domain spectra of the unfocused BNKLT88-1.5Mn and (b) and (c) PZT-841. The simulation results have also been illustrated for comparison with experimental data.

The properties of commercial hard PZT were obtained from [19] and [36]–[41]. BNKLT88-1.5Mn exhibited a mechanical quality factor and dielectric loss comparable with hard PZT. Although, the BNT-based composition shows considerably lower planar coupling coefficient and dielectric constant, its higher coercive field ($E_c = 52$ kV $\cdot$ cm^{-1}) makes it an excellent candidate for high-power applications. The piezoceramic with a higher coercive field shows higher depolarization field and better performance at higher vibration velocity. High-power performance of Mn-doped BNKLT88 composition has comprehensively been studied and can be found in [22]–[24] and [27].

The time-echo responses, frequency spectra, and PiezoCAD results of the unfocused transducers are shown in Fig. 5. The BNT-based transducer [Fig. 5(a) and (c)] exhibited center frequency (f_c) of 3.6 MHz, and −6 dB BW of 19.9%. Evaluation of the pulse-echo waveform of the PZT-based transducer [Fig. 5(b) and (d)] exhibited center frequency (f_c) of 3.9 MHz, and −6 dB BW of 17.95%. Fig. 5 shows a good agreement between simulation and experimental results for both transducers.

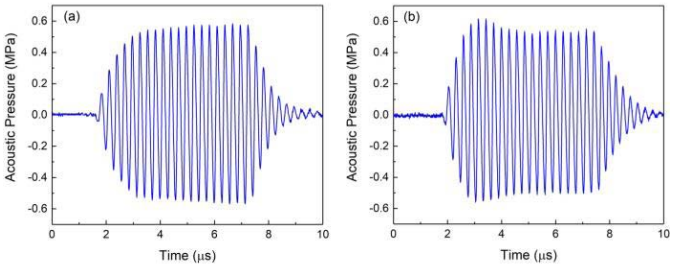

Fig. 6. Acoustic pressure spectrum of (a) BNT-based transducer and (b) PZT-based transducer at the 20 burst count ($n = 20$).

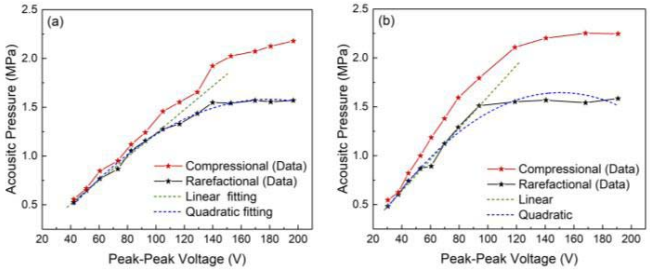

Fig. 7. Compressional and rarefactional acoustic pressure versus peak-to-peak voltage of 3.5 MHz. (a) BNT-based transducer. (b) PZT-based transducer.

The acoustic pressure waveform of both transducers at 20 burst count reached to stable value after four or five cycles as shown in Fig. 6.

Fig. 7 shows the acoustic pressure versus peak-to-peak voltage (V_{pp}) behavior of the transducers. The linear and quadratic regression of rarefactional acoustic (Negative Acoustic) pressure has been used to obtain the starting point of nonlinearity. The rarefactional acoustic pressure of BNT-based transducer shows linear response up to 105 V, where the acoustic pressure was measured to be about 1.13 MPa. The PZT-transducer shows nonlinearity after 70 V with an acoustic pressure of 1.01 MPa. Using (5), the acoustic intensities corresponding to the maximum rarefactional pressure of BNT-based and PZT-based transducer was calculated to be 43 and 34 W/cm^2, respectively. One can conclude that the peak rarefaction pressure of the BNT-based transducer can reach a higher value than the PZT-based transducer.

The probability and threshold for inertial cavitation defines through the concept of the mechanical index (MI)

$$\mathrm{MI} = \frac{P_{r,\mathrm{derated}}}{\sqrt{f_c}} \tag{10}$$

in which the $P_{r,\mathrm{derated}}$ is the derated peak rarefactional pressure (MPa) at the location of the maximum peak intensity integral and f is the frequency (MHz). Food and drug administration mandates the mechanical index to be less than 1.9 for diagnostic transducers. The high value of MI (>0.7) is needed for significant cavitation activity and bioeffects [42].

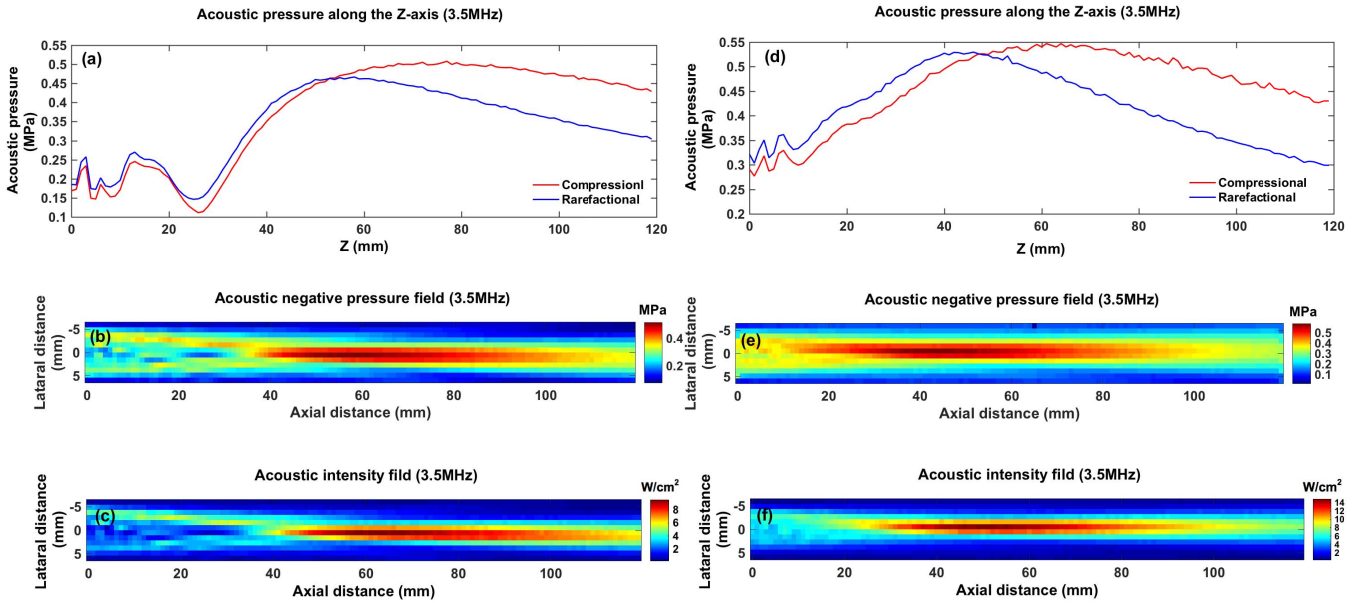

Fig. 8. (a) Acoustic pressure along the z-axis of BNT-based transducer. (b) and (c) 2-D distribution of rarefaction acoustic pressure and acoustic intensity of BNT-based transducer. (d) Acoustic pressure along the z-axis of PZT-based transducer. (e) and (f) 2-D distribution of rarefaction acoustic pressure and acoustic intensity of PZT-based transducer.

TABLE II
ACOUSTIC OUTPUT EXPOSURE LEVELS

	V_{pp} (V)	$P_{r,max}$ (MPa)	I_{sppa} (W/cm^2)		I_{spta} (W/cm^2) (Eq.6)		MI	W_o (mW)
			Exp.	Eq. 5	Exp. I_{sppa}	I_{sppa} from Eq. 5		
BNKLT88-1.5Mn	57	0.52	9.6	9.03	5.5×10^{-3}	5.2×10^{-3}	0.28	0.24
	105	1.13	---	42	---	24.4×10^{-3}	0.60	~1.1
PZT 841	45	0.6	14	12.2	8.6×10^{-3}	7×10^{-3}	0.32	0.35
	70	1.01	---	34	---	19.5×10^{-3}	0.58	~ 0.8

Considering the saturation of rarefactional pressure of BNT-based transducer at V_{pp} of approximately 105 V with the pressure of 1.13 Mpa, the MI can reach to 0.6, depending on the peak-to-peak voltage. In the same way, the mechanical index of the PZT-based transducer can reach to 0.58 at V_{pp} of 70 V. This result suggests that the potential of the BNT-based transducer for inertial cavitation is comparable with the PZT-based transducer.

Fig. 8(a)–(c) shows the 2-D distribution of acoustic pressure and acoustic intensity along z-axis of the BNT-based transducer measured at the peak-to-peak voltage of 57 V. This transducer illustrates maximum rarefactional pressure of 0.52 MPa at about 60 mm from the transducer surface. The near-field and far-field regions of the US beam can be determined from these results [Fig. 8(a)]. The maximum acoustic pressure corresponds to the natural focal point, the transition point from the near-field to the far-field regions, of a flat transducer. The spatial peak pulse average intensity of BNT-based transducer was measured 9.57 W/cm^2 [Fig. 8(c)] and is calculated by (5) as 9.03 W/cm^2. The spatial peak temporal average (I_{spta}) and output power of BNT-based transducer were 5.4×10^{-3} W/cm^2 and 3.2 mW, respectively.

Acoustic pressure and intensity field of the PZT-based transducer at the peak-to-peak voltage of 45 V is presented in Fig. 8(d)–(f). The maximum rarefaction pressure of 0.58 MPa, the spatial peak pulse average of 14.9 W/cm^2, calculated spatial peak temporal average of 8.6×10^{-3} W/cm^2, and the output power of 0.35 mW were obtained at 55-mm distance from the surface of the transducer.

The nonlinearity of the BNT-based transducer occurs at higher V_{pp} compared to PZT-transducer. The BNT-based transducer has higher depolarization field which allows imposing higher operating field. This results in obtaining higher acoustic pressure, acoustic intensity, and output power compared to PZT-transducer. Table II summarizes the acoustic output exposure level of the transducers.

IV. Conclusion

In this paper, the electromechanical properties at room temperature, temperature dependence of dielectric constant, and loss tangent of BNKLT88-1.5Mn have been studied. T_d, T_{R-T}, and T_m of this lead-free BNT-based composition were 205 °C, 220 °C, and 265 °C, respectively. Two different unfocused single-element transducers with a center frequency of 3.5 MHz were fabricated using BNKLT88-1.5Mn and PZT-841 ceramics. BNT-based transducer showed −6 dB BW of 20% which is similar to −6 dB BW of PZT-841 transducer (∼18%). $P_{r,\max}$, I_{sppa}, I_{spta}, and w_o values of the BNT-based transducer measured at the peak-to-peak voltage of 57 V were 0.52 MPa, 9.6 W/cm^2, 5.5×10^{-3} W/cm^2, and 0.24 mW, respectively. In addition, the rarefaction pressure, acoustic intensity, spatial peak temporal average intensity, and output power of lead-free transducer can reach to 1.1 MPa, 42 W/cm^2, 24×10^{-3} W/cm^2, and 1 mW at higher V_{pp}. In the same way, $P_{r,\max}$, I_{sppa}, I_{spta}, and w_o values of PZT-based transducer evaluated at the peak-to-peak voltage of 45 V were 0.58 MPa, 14.9 W/cm^2, 8.6×10^{-3} W/cm^2, and 0.35 mW, respectively. The results of this paper showed that the performance of BNT-based transducer were comparable with PZT-based one.

References

[1] L. D. Sullivan, M. G. McLoughlin, L. G. Goldenberg, M. E. Gleave, and K. W. Marich, "Early experience with high-intensity focused ultrasound for the treatment of benign prostatic hypertrophy," *BJU Int.*, vol. 79, no. 2, pp. 172–176, Feb. 1997.

[2] T. Uchida, M. Muramoto, H. Kyunou, M. Iwamura, S. Egawa, and K. Koshiba, "Clinical outcome of high-intensity focused ultrasound for treating benign prostatic hyperplasia: Preliminary report," *Urology*, vol. 52, no. 1, pp. 66–71, Jul. 1998.

[3] C. Chaussy and S. Thüroff, "The status of high-intensity focused ultrasound in the treatment of localized prostate cancer and the impact of a combined resection," *Current Urol. Rep.*, vol. 4, no. 3, pp. 248–252, May 2003.

[4] S. Thüroff *et al.*, "High-intensity focused ultrasound and localized prostate cancer: Efficacy results from the European multicentric study," *J. Endourol.*, vol. 17, no. 8, pp. 673–677, Oct. 2003.

[5] C. Chaussy and S. Thüroff, "High-intensity focused ultrasound in prostate cancer: Results after 3 years," *Mol. Urol.*, vol. 4, no. 3, pp. 179–182, 2000.

[6] T. Uchida *et al.*, "Five years experience of transrectal high-intensity focused ultrasound using the Sonablate device in the treatment of localized prostate cancer," *Int. J. Urol.*, vol. 13, no. 3, pp. 228–233, Mar. 2006.

[7] A. Blana, B. Walter, S. Rogenhofer, and W. F. Wieland, "High-intensity focused ultrasound for the treatment of localized prostate cancer: 5-year experience," *Urology*, vol. 63, no. 2, pp. 297–300, Feb. 2004.

[8] H. Furusawa *et al.*, "The evolving non-surgical ablation of breast cancer: MR Guided focused ultrasound (MRgFUS)," *Breast Cancer*, vol. 14, no. 1, pp. 55–58, Jan. 2007.

[9] F. Wu *et al.*, "Extracorporeal high intensity focused ultrasound treatment for patients with breast cancer," *Breast Cancer Res. Treat.*, vol. 92, no. 1, pp. 51–60, Jul. 2005.

[10] S. D. LeBlang, K. Hoctor, and F. L. Steinberg, "Leiomyoma shrinkage after MRI-guided focused ultrasound treatment: Report of 80 patients," *Amer. J. Roentgenol.*, vol. 194, no. 1, pp. 274–280, Jan. 2010.

[11] K. Funaki, H. Fukunishi, and K. Sawada, "Clinical outcomes of magnetic resonance-guided focused ultrasound surgery for uterine myomas: 24-month follow-up," *Ultrasound Obstetrics Gynecol.*, vol. 34, no. 5, pp. 584–589, Nov. 2009.

[12] C.-X. Li *et al.*, "Analysis of clinical effect of high-intensity focused ultrasound on liver cancer," *World J. Gastroenterol.*, vol. 10, no. 15, pp. 2201–2204, Aug. 2004.

[13] F. Wu, Z.-B. Wang, W.-Z. Chen, J. Bai, H. Zhu, and T.-Y. Qiao, "Preliminary experience using high intensity focused ultrasound for the treatment of patients with advanced stage renal malignancy," *J. Urol.*, vol. 170, no. 6, pp. 2237–2240, Dec. 2003.

[14] F. Wu *et al.*, "Feasibility of US-guided high-intensity focused ultrasound treatment in patients with advanced pancreatic cancer: Initial experience," *Radiology*, vol. 236, no. 3, pp. 1034–1040, Sep. 2005.

[15] B. Liberman *et al.*, "Pain palliation in patients with bone metastases using mr-guided focused ultrasound surgery: A multicenter study," *Ann. Surg. Oncol.*, vol. 16, no. 1, pp. 140–146, Nov. 2008.

[16] Y.-F. Zhou, "High intensity focused ultrasound in clinical tumor ablation," *World J. Clin. Oncol.*, vol. 2, no. 1, pp. 8–27, Jan. 2011.

[17] D. G. ter Haar and C. Coussios, "High intensity focused ultrasound: Physical principles and devices," *Int. J. Hyperthermia*, vol. 23, no. 2, pp. 89–104, Jan. 2007.

[18] H. J. Lee, S. O. Ural, L. Chen, K. Uchino, and S. Zhang, "High power characteristics of lead-free piezoelectric ceramics," *J. Amer. Ceram. Soc.*, vol. 95, no. 11, pp. 3383–3386, Nov. 2012.

[19] S. Zhang, J. B. Lim, H. J. Lee, and T. R. Shrout, "Characterization of hard piezoelectric lead-free ceramics," *IEEE Trans. Ultrason., Ferroelect., Freq. Control*, vol. 56, no. 8, pp. 1523–1527, Aug. 2009.

[20] T. Tou, Y. Hamaguti, Y. Maida, H. Yamamori, K. Takahashi, and Y. Terashima, "Properties of $(Bi_{0.5}Na_{0.5})TiO_3$–$BaTiO_3$–$(Bi_{0.5}Na_{0.5})(Mn_{1/3}Nb_{2/3})O_3$ lead-free piezoelectric ceramics and its application to ultrasonic cleaner," *Jpn. J. Appl. Phys.*, vol. 48, no. 7S, p. 07GM03, Jul. 2009.

[21] E. Taghaddos, M. Hejazi, and A. Safari, "Electromechanical properties of acceptor-doped lead-free piezoelectric ceramics," *J. Amer. Ceram. Soc.*, vol. 97, no. 6, pp. 1756–1762, Jun. 2014.

[22] M. Hejazi, E. Taghaddos, E. Gurdal, K. Uchino, and A. Safari, "High power performance of manganese-doped BNT-based Pb-free piezoelectric ceramics," *J. Amer. Ceram. Soc.*, vol. 97, no. 10, pp. 3192–3196, Oct. 2014.

[23] H. Nagata, K. Takai, Y. Nomura, S. Sato, Y. Hiruma, and T. Takenaka, "Vibration velocities under high-power driving on perovskite-type lead-free ferroelectric ceramics," in *Proc. IEEE Int. Symp. Appl. Ferroelectr. (ISAF)*, Aug. 2010, pp. 1–4.

[24] Y. Hiruma, H. Nagata, and T. Takenaka, "Phase-transition temperatures and piezoelectric properties of $(Bi_{1/2}Na_{1/2})TiO_3$-$(Bi_{1/2}Li_{1/2})TiO_3$-$(Bi_{1/2}K_{1/2})TiO_3$ lead-free ferroelectric ceramics," *IEEE Trans. Ultrason., Ferroelect., Freq. Control*, vol. 54, no. 12, pp. 2493–2499, Dec. 2007.

[25] Y. Gao, Y.-H. Chen, J. Ryu, K. Uchino, and D. Viehland, "Eu and Yb substituent effects on the properties of $Pb(Zr_{0.52}Ti_{0.48})O_3$–$Pb(Mn_{1/3}Sb_{2/3})O_3$ ceramics: Development of a new high-power piezoelectric with enhanced vibrational velocity," *Jpn. J. Appl. Phys.*, vol. 40, no. 2A, pp. 687–693, Feb. 2001.

[26] S. O. Ural, Y. Zhuang, S. Tuncdemir, and K. Uchino, "Comparison of power density characteristics among disk and plate shaped piezoelectric devices," *Jpn. J. Appl. Phys.*, vol. 49, no. 2R, p. 021502, Feb. 2010.

[27] T. Takenaka, H. Nagata, and Y. Hiruma, "Phase transition temperatures and piezoelectric properties of $(Bi_{1/2}Na_{1/2})TiO_3$-and $(Bi_{1/2}K_{1/2})TiO_3$-based bismuth perovskite lead-free ferroelectric ceramics," *IEEE Trans. Ultrason., Ferroelect., Freq. Control*, vol. 56, no. 8, pp. 1595–1612, Aug. 2009.

[28] Z.-Y. Shen, J.-F. Li, R. Chen, Q. Zhou, and K. K. Shung, "Microscale 1–3-type $(Na,K)NbO_3$-based Pb-free piezocomposites for high-frequency ultrasonic transducer applications," *J. Amer. Ceram. Soc.*, vol. 94, no. 5, pp. 1346–1349, May 2011.

[29] M. M. Hejazi, B. Jadidian, and A. Safari, "Fabrication and evaluation of a single-element $Bi_{0.5}Na_{0.5}TiO_3$-based ultrasonic transducer," *IEEE Trans. Ultrason., Ferroelect., Freq. Control*, vol. 59, no. 8, pp. 1840–1847, Aug. 2012.

[30] A. H. Meitzler (Chairman), D. Berlincourt, G. A. Coquin, F. S. Welsh, III, H. F. Tiersten, and A. W. Warner, "Publication and proposed revision of ANSI/IEEE standard 176–1987 'ANSI/IEEE standard on piezoelectricity,"' *IEEE Trans. Ultrason., Ferroelect., Freq. Control*, vol. 43, no. 5, p. 717, Sep. 1996.

[31] M. S. Canney, M. R. Bailey, L. A. Crum, V. A. Khokhlova, and O. A. Sapozhnikov, "Acoustic characterization of high intensity focused ultrasound fields: A combined measurement and modeling approach," *J. Acoust. Soc. Amer.*, vol. 124, no. 4, pp. 2406–2420, Oct. 2008.

[32] C. R. Hill, "Optimum acoustic frequency for focused ultrasound surgery," *Ultrasound Med. Biol.*, vol. 20, no. 3, pp. 271–277, Jan. 1994.
[33] S. B. Barnett and G. Kossoff, "Temporal peak intensity as a critical parameter in ultrasound dosimetry," *J. Ultrasound Med.*, vol. 3, no. 9, pp. 385–389, Sep. 1984.
[34] Y. Hiruma, H. Nagata, and T. Takenaka, "Phase transition temperatures and piezoelectric properties of $(Bi_{1/2}Na_{1/2})TiO_3$–$(Bi_{1/2}K_{1/2})TiO_3$ –$BaTiO_3$ lead-free piezoelectric ceramics," *Jpn. J. Appl. Phys.*, vol. 45, no. 9B, pp. 7409–7412, Sep. 2006.
[35] E.-M. Anton, W. Jo, D. Damjanovic, and J. Rödel, "Determination of depolarization temperature of $(Bi_{1/2}Na_{1/2})TiO_3$-based lead-free piezoceramics," *J. Appl. Phys.*, vol. 110, no. 9, p. 094108, Nov. 2011.
[36] T. R. Shrout and S. J. Zhang, "Lead-free piezoelectric ceramics: Alternatives for PZT?" *J. Electroceram.*, vol. 19, no. 1, pp. 113–126, Feb. 2007.
[37] M. W. Hooker, "Properties of PZT-Based Piezoelectric Ceramics Between −150 and 250 C," NASA, Washington, DC, USA, Tech. Rep. NASA/CR-1998-208708, Sep. 1998.
[38] *Piezoelectric Materials Datasheet. Piezopower*, CTS Electron. Compon. Co., Albuquerque, NM, USA. [Online]. Available: https://www.ctscorp.com/wp-content/uploads/CTS-Corporation-Piezoelectric-Material-Manufacturer-Ceramic-Polycrystalline-Materials.pdf
[39] *Piezomaterial Data, Specific Parameters of Standard Materials*. PI Ceramics Co., Lederhose, Germany. [Online]. Available: https://static.piceramic.com/fileadmin/user_upload/physik_instrumente/files/datasheets/PI_Ceramic_Material_Data.pdf
[40] *Piezoelectric Ceramics Datasheet*, Morgan Adv. Mater., Berkshire, U.K.
[41] *Physical and Piezoelectric Properties of APC Materials*, APC Int., Ltd., West Kingston, RI, USA. [Online]. Available: https://www.americanpiezo.com/apc-materials/physical-piezoelectric-properties.html
[42] Center for Devices and Radiological Health, "Guidance for industry and FDA staff—Information for manufacturers seeking marketing clearance of diagnostic ultrasound systems and transducers," Center Devices Radiol. Health, Rockville, MD, USA, Sep. 2008. [Online]. Available: https://www.fda.gov/downloads/UCM070911.pdf

Elaheh Taghaddos received the B.S. degree in materials science and engineering in 2005, and the M.S. degree in materials science and engineering from Rutgers University, New Brunswick, NJ, USA, in 2017, where she is currently pursuing the Ph.D. degree in material science and engineering.

She was with the Iranshir Company, Qazvin, Iran, as a Project Manager, and then joined Glenn Howatt Electroceramics Laboratories, Rutgers University, as a Visiting Scientist. She has been involved in the development of hard bismuth sodium titanate (BNT)-based compositions and ultrasonic transducers for therapeutic applications. Her research interests include synthesize, fabrication, and characterization of lead-free ferroelectric materials in the form of ceramics, thin films, nanowires, and composites.

T. Ma, photograph and biography not available at the time of publication.

Hui Zhong was born in Xi'an China, in 1977. She received the B.S. and Ph.D. degrees in biomedical engineering from Xi'an Jiaotong University, Xi'an, China, in 2000 and 2006, respectively.

She is currently a Lecturer with the Department of Biomedical Engineering, Xi'an Jiaotong University. Her current research interests include ultrasound imaging for monitoring thermal ablation and cavitation in HIFU therapy.

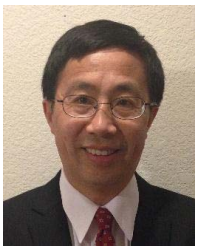

Qifa Zhou received the Ph.D. degree from the Department of Electronic Materials and Engineering, Xi'an Jiaotong University, Xi'an, China, in 1993.

He is currently a Professor of Ophthalmology and Biomedical Engineering with the University of Southern California (USC), Los Angeles, CA, USA. Before joining USC in 2002, he was with the Department of Physics, Sun Yat-Sen University, Guangzhou, China, the Department of Applied Physics, Hong Kong Polytechnic University, Hong Kong, and the Materials Research Laboratory, Pennsylvania State University, State College, PA, USA. He is actively exploring ultrasonic mediated therapeutic technology including trans-sclera drug delivery, and ultrasound for retinal and brain stimulation. He has authored over 200 peer-reviewed articles in journals including *Nature Medicine, Nature Communication, Advanced Materials*, and IEEE TRANSACTIONS ON ULTRASONICS, FERROELECTRICS, AND FREQUENCY CONTROL. His research focuses on the development of piezoelectric high-frequency ultrasonic transducers for biomedical ultrasound and photoacoustic imaging, including intravascular imaging, cancer imaging, and ophthalmic imaging.

Dr. Zhou is a member of the Technical Program Committee of the IEEE International Ultrasonics Symposium. He is a fellow of the International Society for Optics and Photonics and the American Institute for Medical and Biological Engineering. He is an Associate Editor of the IEEE TRANSACTIONS ON ULTRASONICS, FERROELECTRICS, AND FREQUENCY CONTROL.

M. X. Wan, photograph and biography not available at the time of publication.

Ahmad Safari is currently a Distinguished Professor and the Director of the Glenn Howatt Laboratory, Department of the Materials Science and Engineering, Rutgers University, New Brunswick, NJ, USA.

He has advised over 25 Ph.D. students and worked with over 30 Post-Doctoral Research Associates. He has edited a book, authored over 400 book chapters and journal articles, and holds 22 U.S. patents. His research interest is in structural-property relationship in dielectric, multiferroic, and piezoelectric thick and thin films, ceramics and composite for transducers, sensors, and energy harvesting and 3-D printing of novel design of advanced functional materials.

Dr. Safari is a fellow of the IEEE-UFFC Society and the American Ceramic Society and a member of the World Academy of Ceramics. He has been awarded the IEEE-UFFC Robert E. Newnham Ferroelectrics, Ferroelectrics Recognition, and Distinguished Service Awards and he is a recipient of the U.S.-Japan Electro-Ceramic Bridge Building Award. At Rutgers, he has been named Jacob Chair in Applied Physics. He has served the IEEE-UFFC Society in variety of key positions including president of the society and general chair of 2013 joint IEEE-UFFC-EFTF-PFM Conference in Prague.